JAAS

PAPER

View Article Online
View Journal | View Issue

Cite this: *J. Anal. At. Spectrom.*, 2022, **37**, 2383

High resolution off resonant spectroscopy as a probe of the oxidation state†

Michal Nowakowski, *[a] Aleksandr Kalinko, [b] Jakub Szlachetko, [c] Rafał Fanselow [d] and Matthias Bauer [a]

Currently, chemistry and physics are strongly dependent on the concept of the oxidation state. While the formal oxidation state is easily evaluated, the real physical oxidation state value is often difficult to determine and significantly varies from the formal values. Determination of the ionization threshold in X-ray absorption spectroscopy (XANES) relies on the absorption edge position and sometimes poses limitations, mainly due to the edge resonances. Moreover, the lower energy states can be probed only within x-soft or XUV photons providing only surface state information of probed materials. Here, we employ high energy resolution off-resonant spectroscopy to determine both 1s and 3p binding energies of Fe-based materials and therefore correlate to their physical oxidation state. The results are compared to the ones obtained with classical X-ray absorption, X-ray emission, and photoelectron spectroscopies. The observed differences in binding energies are discussed in a frame of initial and final state interactions with the atom's electronic configurations. The presented methodology is discussed towards potential use to single-shot experiments and application at X-ray free-electron lasers. Alternatively, core level X-ray emission spectroscopy can be used, but the emission line positions are strongly affected by spin-orbit interaction. However, due to the energy transfer from the photon to the excited core electron, the same information as in XANES is probed in high energy resolution off-resonant spectroscopy (HEROS). Based on the Kramers–Heisenberg theory, we propose a new approach for ionization threshold determination which is free of the limitations encountered in XANES-based determination of the core state energy. Namely, the value of core state energy can be determined analytically using a few HEROS spectra recorded with significantly higher spectral resolution. This approach provides a basis for the universal physical oxidation state determination method.

Received 5th July 2022
Accepted 26th September 2022

DOI: 10.1039/d2ja00232a

rsc.li/jaas

Introduction

Electronic structure determination of chemical complexes employing hard X-ray spectroscopy is an ongoing challenge. While most of the definitions and conventions are unambiguous, the definition of fundamental oxidation states is based on textbook formalism. Numerous attempts to assign physical oxidation states based on spectroscopic approaches exist.[1–3] While covalent compounds with synergistic donor and acceptor bonds remain a significant challenge,[4] ionic compounds are intrinsically more suited to establish experimental methods for oxidation state determination.

A canonical way to assign an oxidation state is to use X-ray absorption spectroscopy (XAS). The method is based on photoexcitation of core-level electrons above the Fermi level of a compound, and in simple understanding, the absorption coefficient is proportional to the density of unoccupied states (unoccupied DOS). XAS theory, instrumentation, and applications are well described in the literature and textbooks.[5–11] In K-edge spectroscopy of 3d metal compounds, the electron is excited from a $1s^2$ state resulting in a $1s^1\varepsilon p$ final state (superscript represents the number of electrons). In simple electrostatic terms, the absorption edge sensitivity to the oxidation state can be explained as the difference in electrostatic potential between the non-ionized N electron and the N-1 electron system. The energy required for photoexcitation of the 1s electron will be lower for the N-electron system since the total core potential is less negative than in the N-1 electron system. Thus, the edge position for the N-electron system will be observed at smaller energies compared to that for the N-1 electron system.[12,13] Alternatively, the 1s → 4p transition (to continuum, with a limited lifetime) energy is used to correlate the metal-ligand bond distance (R) to the oxidation state. In simple

[a]Department Chemie, Universität Paderborn, Warburger Str. 100, 33098 Paderborn, Germany. E-mail: michal.nowakowski@upb.de
[b]Deutsches Elektronen-Synchrotron DESY, Notkestr. 85, 22607 Hamburg, Germany
[c]SOLARIS National Synchrotron Radiation Centre, Jagiellonian University, Krakow 30-392, Poland
[d]Institute of Nuclear Physics Polish Academy of Sciences, Kraków, 31-342, Poland

† Electronic supplementary information (ESI) available. See https://doi.org/10.1039/d2ja00232a

compounds the distance gets shorter for a higher oxidation state, and the energy of the 4p acceptor state rises by a factor of R^{-2} relative to the ionization threshold.[14] The edge position is higher in energy for a higher oxidation state in both cases. K-edge X-ray absorption near edge structure (XANES) of transition metals (TM) is based on 1s → np transition ($n = 3,4,5$), and the position of the inflection point of the rising edge is used as a measure for the ionization threshold.[15] The edge position can be determined experimentally from the maximum of the I^{st} or zero value of the II^{nd} derivative. Unfortunately, XANES or high energy resolution fluorescence detected (HERFD) XANES[16] are often heavily affected by ligand contributions in the rising edge.[17,18] The presence of additional transitions (1s → 3d, 1s → $2p_{Lignad}$, and 1s → 4p) in the edge region that have intrinsic lifetimes and experimental broadening leads to ambiguities.[19] Although carefully selected references can sometimes account for these, more often than not, they hinder precise oxidation state determination. In many cases, for example for Mn contamination in air, a linear combination fitting (LCF) analysis of XANES spectra allowed the determination of the oxidation state of compounds in the pollution mixture.[20] The fingerprinting property of near-edge was also demonstrated for Cu in determination of the oxidation state of reagents in catalytic reactions *via* LCF.[21] However, the method is limited for the cases where feasible references with similar electronic structure are available. In such cases, uncertainties are mostly arising from spectral intensities, precision of energy calibration curves, energy resolution and experimental stability. The final error bar for the oxidation state obtained by the LCF procedure is amplified by the aforementioned factors and fitting procedure giving rise to values between 10 and 20%. In some geologic and analytic studies, the problem of the edge position was circumvented by using the intrinsic sensitivity of the pre-edge feature to determine the oxidation state solely or in cross-reference with Mössbauer spectroscopy.[22–26]

Complementary to XAS, X-ray emission spectroscopy (XES) can be used to get more insight into the electronic structure of an atom. While the physical principles are the same as in XAS, the method is focused on occupied densities of states from which a created core hole is filled, resulting in a fluorescence decay channel. For 3d transition metals, the analysis of the core-to-core (CtC) Kβ XES mainline, described by a $1s^13p^63d^n \rightarrow 1s^23p^53d^{n+1}$ transition is the method of choice for the oxidation state determination in the limit of K edge excitation. The resulting spectrum is broadened by the initial and final lifetimes. The presence of unpaired 3d electrons induces additional 3p–3d exchange interaction that lifts the 3d state degeneration and leads to an additional split in the mainline accompanied by the appearance of a satellite Kβ′ peak.[27–29] The energy difference between Kβ and Kβ′ lines which describes the energy distinction between high- and low-spin states and is denoted in spin-orbit coupling theory, changes with the number of unpaired 3d electrons (spin multiplicity) and the oxidation state.[30] The position of the Kβ mainline is affected by spin-orbit coupling and the valence shell angular momentum, causing an entangled nature of all interactions.[19] Moreover, the Kβ mainline position is influenced by the ligand field, and the corresponding charge transfer to a metal center frequently referred to as covalency.[29] A localized nature of CtC-XES is considered allowing an oxidation state determination in simple compounds[31–33] and more complex systems[34,35] similar to XANES spectroscopy; the mentioned influences also cause some uncertainties here.

Despite these difficulties and disadvantages of XANES and CtC-XES, a precise oxidation state determination is of the utmost importance in numerous disciplines, like understanding chemical reactivity and electronic structures. Here, the formal oxidation state is defined as the charge of an atom if all of its bonds were fully ionic, while the physical oxidation state represents the 'real' charge on the atom, which is affected by the nature of the chemical bonding. Hard X-ray K-edge spectroscopy offers unique properties to understand chemical systems under realistic conditions, like high pressures and temperatures; thus, a more precise oxidation state determination is highly desired. Resonant X-ray emission spectroscopy (RXES), frequently referred to as RIXS (resonant inelastic X-ray scattering),[36–39] offers new approaches here. RXES is a coherent process in which an electron is excited to a localized state above the Fermi level with near-simultaneous emission of a fluorescence photon.[19,40] The fluorescence emission from a narrow bandwidth (*i.e.* 1 eV) is recorded with varied incident beam energy efficiently discriminated by energy dispersive analyzing crystals. The two-dimensional information on incidence and emission energies allows for spectral analysis with lifetime broadening being reduced significantly.[19] RXES therefore provides highly resolved, complete information on the electronic structure of compounds in the form of a 2D matrix of internally calibrated XAS and XES spectra.[41] Information about unoccupied and occupied electronic states can be derived by performing integration along the vertical and horizontal axes over selected regions of interest, respectively. The RXES plane can be divided into three regions dominated by different physical processes:[42] Off-resonant-, resonant-, and non-resonant XES (high resolution off-resonant spectroscopy XES or HEROS-XES, RXES, and nXES). The main difference between *n*XES and RXES is that in nXES the emission is retarded which results in lost coherence of the process. In such a case, a 1s core electron is photoexcited to the continuum (1s > εp), while in RXES it is photoexcited to the lowest unoccupied levels. On the other hand, in HEROS the excited electron is directly involved in the decay process.[41] In the case of Kβ RXES of 3d metals, the lowest final state will be $1s^23p^53d^{n+1}$. Recently, RXES was proposed as a tool for oxidation state analysis, and there were certain improvements of significant value[34] however, not beyond the already established know-how of the method.[19,37] The excitations in the resonant regime are an impeccable tool for identifying the electronic states and interactions contributing to the physical oxidation state, yet they do not provide a way to quantify this value. This paper aims to demonstrate off-resonant spectroscopy application to determine the ionization threshold value for an atom experimentally. The absorption threshold is understood here in accordance with the International Union of Crystallography definition, as an

energy of the first allowed transition in the absorption spectrum.[43] Thus, similar to the XAS-based experiment, we want to establish HEROS as a tool for precise and sample environment-independent physical oxidation state measurement.

Materials and methods

Experimental details

HEROS and RXES measurements were conducted at the P64 undulator beamline at PETRA III, DESY.[44] A Si(111) double crystal monochromator (DCM) was used for energy selection while beam focusing and harmonic rejection were achieved using cylindrical Si mirrors. The estimated flux on a sample was 10^{13} ph per s. The signal acquisition in wavelength-dispersive mode was made using a von Hamos emission spectrometer[45] equipped with eight Si(440) analyzer crystals. A Pilatus 100 k position-sensitive detector under normal conditions was used for signal detection. The incident energy resolution $\Delta E/E$ was 2×10^{-4}, and the beam spot size on the sample was 100×300 μm^2 (V × H). The DCM calibration was performed using the first inflection point in the Fe foil XAS spectrum set to 7112 eV. The total experimental resolution, including beam, sample, and spectrometer contributions, was determined by using the FWHM value of the elastic peak fitted by using a Gaussian function independently for each sample. The commercial FeS, α-Fe_2O_3 nanopowder, and $FeCl_3$ samples (all purchased from Sigma-Aldrich and used without further purification) were measured as powders enclosed in two layers of Kapton. First, the Kβ RXES planes were recorded (Fig. 1 for $FeCl_3$). Afterward, off-resonant spectra were collected with longer accumulation times for the selected incident energies.

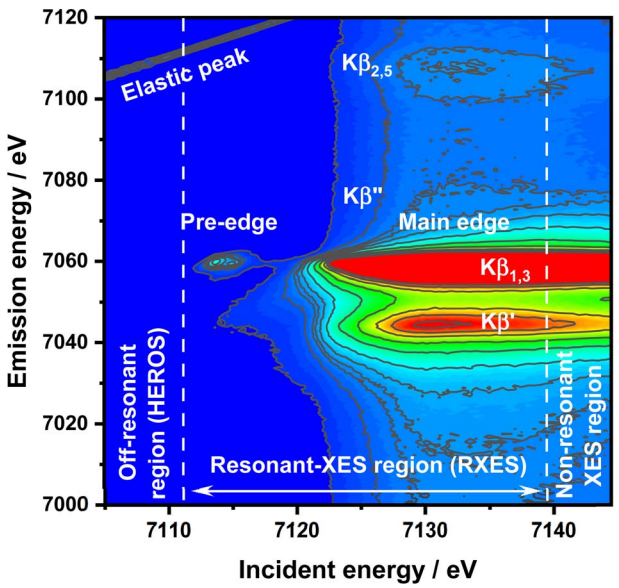

Fig. 1 RXES plane of $FeCl_3$ with all important features and HEROS, RXES, and nXES regions marked.

Off-resonant spectroscopy

For an incident X-ray beam energy tuned significantly below the ionization threshold of an atom, a different physical effect compared to excitations in a resonant regime will occur, leading to the new spectroscopic method, high resolution off resonant spectroscopy (HEROS).[46–50] Like RXES, HEROS is a coherent scattering process with additional instant energy transfer from the emitted photon to the excited electron. It is possible due to energy conservation for the scattering process at a given energy loss E : $E_{em}(E) = E_{inc} - E_f - E$, where E_{em} is the emission energy, E_{inc} is the incident energy, and E_f is the final state energy. In a simple understanding of the K-edge example, the excitation occurs on the Lorentzian tail of the 1s state. During excitation of the electron above the Fermi level by the incoming energy $E_{inc} < E_K$, the remaining energy is transferred from the emitted fluorescence photon (E_{em}) to the excited electron in the quasi-simultaneous process. Therefore, the energy of the emitted photon is reduced by the value of energy transferred to the electron excited above the Fermi level. The following points make HEROS an attractive alternative to conventional XAS or HERFD: (1) the incoming beam energy defines the emission energy; (2) both incoming beam and emitted radiations are below the ionization threshold; (3) fluorescence can be measured with fixed optical geometry and with one incident energy. Due to the mentioned properties, a HEROS spectrum is proportional to the unoccupied density of states, and is free of self-absorption effects.[49] Moreover, the fixed setup for HEROS accumulation makes it a good candidate for time-resolved, shot-to-shot studies, of which proof-of-concept measurements were already demonstrated for $Pt(acac)_2$ thermal decomposition.[51] The limitation of HEROS applications to 3d metal compounds is a low cross-section for the process resulting in two-three orders of magnitude smaller signals than for RXES.[42] This limitation can be circumvented by sufficiently long signal acquisition, increased concentration of the absorber or by performing experiments at brighter sources. With decreasing radiation decay channel yield for elements with $Z < 20$ at the expense of non-radiative decay channels, the relatively low cross-sections of the off-resonant scattering will make the measurements impossible. On the other hand, 5d elements exhibit significantly stronger HEROS signals regarding the emission mainline than 3d elements.[52] Moreover, the HEROS-like scattering signal is visible for incident energies above the absorption edge, and in the case of 3d elements, this scattering is covered by the intense emission mainline. The scattering signal above the resonance is visible, especially in the constant energy transfer RXES plane at the pre-edge resonance. The RXES planes for Fe_2O_3, and FeS are available in the ESI,† while the RXES plane for $FeCl_3$ is shown in Fig. 1. With a proper intensity scale adjustment one could see that HEROS signal features originate from the constant energy transfer contributions that shift continuously with the incident energy.

The principles of HEROS can be explained based on the generalized Kramers–Heisenberg equation derived by Tulkki and Åberg describing the double differential cross-section for the resonant inelastic X-ray scattering.[37,53–55] The equation

describes scattering as a two-stage mechanism: absorption of a photon by the initial atomic state leading to an intermediate state and deexcitation to the final state within the atomic lifetime. The interference between the initial and final configurations can be neglected for hard X-ray energies in a coherent process.[42,53,54] The assumption that the oscillator strength describing the excitation above the Fermi level is proportional to the unoccupied DOS functions and intensity of the emitted fluorescence to the cross-section will allow to simplify the equation and rewrite it for given photoelectron energy[49] in the case of the Kβ emission line region for 3d metals. The lifetime of the final state is neglected and replaced by a Dirac delta function to maintain energy conservation.[49–51,56] The integral can be calculated analytically, using the relation $E_{em} = E_{inc} - |E_{M3}| - E$ for the integral solution, and the result will be as follows:[50]

$$I_{XES}(E_{em}) \propto \frac{E_{em}}{E_{inc}} \frac{(|E_K| - |E_{M3}|)(E_{inc} - E_{em} - |E_{M3}| + |E_K|)}{(|E_K| - E_{em} - |E_{M3}|)^2 + \Gamma_K^2/4}$$

$$I_{XAS}(E_{inc} - E_{em} - |E_{M3}|) \quad (1)$$

where $I_{XES}(E_{em})$ and $I_{XAS}(E)$ are the intensities of the XES and XAS spectrum, respectively, E_K and E_M3 are the initial ($1s^2 3p^6 4p^0$) and final states ($1s^2 3p^5 4p^1$), and Γ_K is the initial state broadening. Eqn (1) gives a simple analytical relation between XAS and XES in the off-resonant regime, enabling the interconversion of both sets of spectral data. We should note that the measured off-resonant XES will indeed represent the convolution of the distribution of the final state with the XAS function. Accordingly, XAS intensities can be determined based on a given off-resonant XES spectrum. The example for three iron compounds is shown in Fig. 2, where HEROS-XES to HEROS-XAS transformation was conducted according to eqn (1). The energy scale was set relative to the E_K level.[57] There are few limitations for direct application of eqn (1) for the HEROS-XES to HEROS-XAS transition in oxidation state determination.

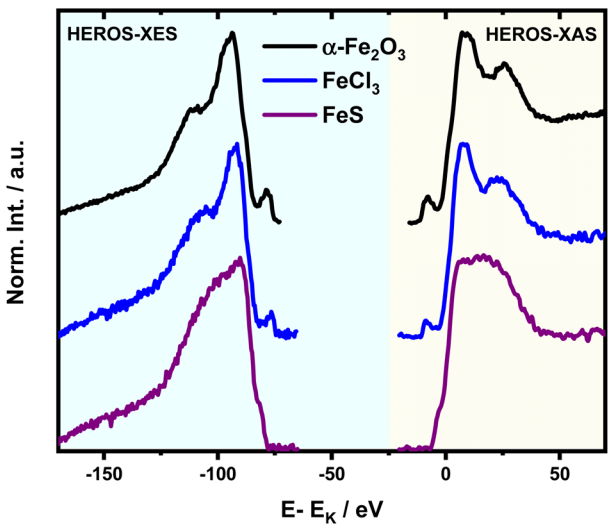

Fig. 2 HEROS-XES to HEROS-XAS transition according to eqn (1) for all studied references performed on spectra recorded at an incident energy of 7100 eV.

It is important to underline that determination of XAS from HEROS through eqn (1) will work only for the incidence beam energies set below the absorption threshold, *i.e.*, under conditions far away of resonances. The critical factor that governs HEROS is detuning, *i.e.*, the $E_K - E_{inc}$ value, with the condition that $E_K > E_{inc}$, which can be formulated using the detuning parameter $\delta E = E_K - E_{inc}$. Fig. 3 presents the impact of detuning δE on the shape and intensities of the HEROS-XES spectra for $FeCl_3$ for selected incident energies below the absorption edge. $FeCl_3$ HEROS-XES spectra were recorded for incident energies of

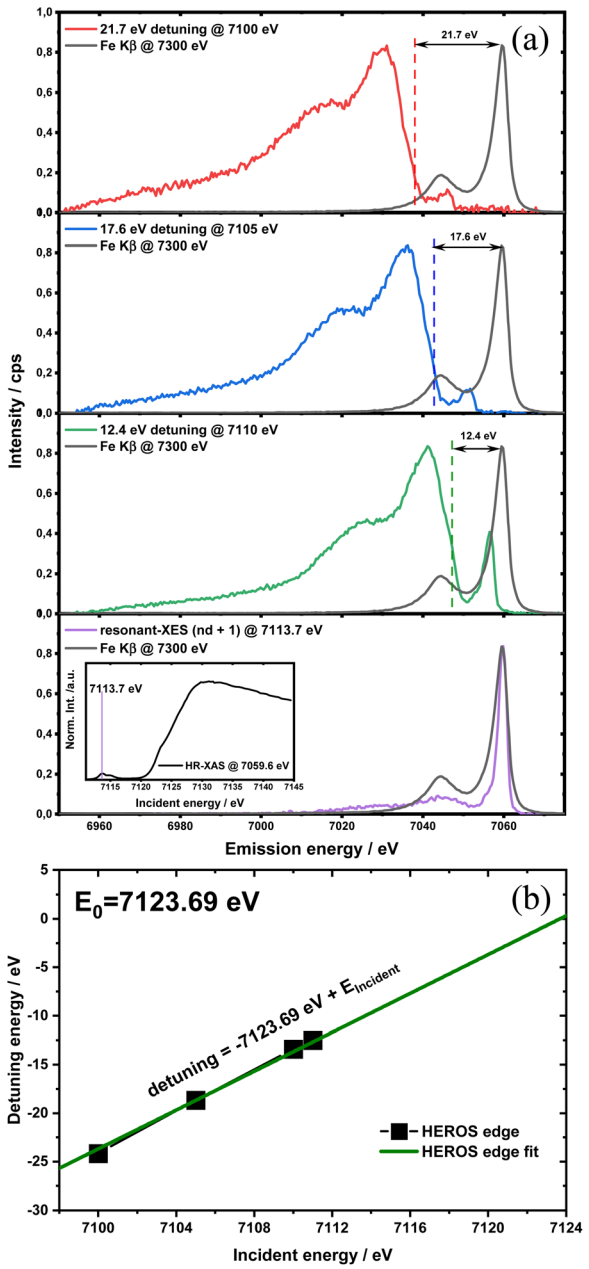

Fig. 3 (a) Detuning parameter δE in the function of incident energy and position changes of HEROS spectra with respect to nXES for $FeCl_3$. The inset shows an incident energy of 7113.7 eV on the HR-XAS spectrum (@7059.6 eV) for which a resonant-XES spectrum was collected; (b) $\delta E(E_{inc})$ relation with extrapolation to $\delta E = 0$.

7100–7113.7 eV and compared to the position of the $K\beta_{1,3}$ mainline. The dashed lines represent a high energy cut-off ($E_{cut-off}$) of the off-resonant spectra. While for 7100 eV and 7105 eV, HEROS spectra have a similar shape and shifted energy positions, for $\delta E = -12.4$ eV ($E_{inc} = 7110$ eV), the HEROS-XES is already significantly affected by the presence of the RXES $K\beta_{1,3}$ line, namely at the HEROS pre-edge peak at 7056 eV. Notably, the edge position in the HEROS-XAS spectra after transformation is always at a defined value, while the high energy cut-off position in HEROS-XES will depend on the detuning parameter, and so, on the employed incidence beam energy. On the other hand, energy scales of reconstructed XAS spectra from off-resonant data will be affected by significant uncertainty since eqn (1) requests to precisely define the E_K and E_{M3} energies, while they are oxidation-state dependent. The same behavior is found for other Fe compounds measured in the current experiment: FeS and α-Fe_2O_3, and the corresponding results are shown in the ESI.† However, we should stress that the relative energies of cut-off positions in HEROS can be determined with high precision. This property and the linear behavior determined by the universal law given by eqn (1) offers a new way for the precise determination of E_{1s} and thus, of the physical oxidation state. The calibration procedure requires the tuning of monochromator energy to match the inflection point of the metal foil absorption spectrum to the reference value. Using the HEROS and δE definition, the measured value is a difference between $E_{cut-off}$ and E_{M3}. It will allow the determination of the absorption edge position E_K using only HEROS-XES spectra in a fixed XES setup. Given the strong X-ray fluorescence signals the Compton scattering contribution is negligible under applied experimental conditions due to the low cross-section.[58]

Results and discussion

HEROS-XES probes a convoluted final state distribution with an unoccupied density of states, and the high energy cut-off relates to E_K in XAS *via* energy conservation for the scattering process. The HEROS-XES edge (high energy cut-off) can be defined as $E_{cut-off} = E_K - \delta E - E_{M3}$, where δE is the detuning energy of the incoming X-rays with respect to the 1s threshold energy. Since δE equals $E_{inc} - E_K$, the HEROS-XES cut-off can simply be defined as E_{inc}–E_{M3}. The energy conservation of the scattering process under off-resonant conditions can be used to determine the position of E_{1s} from the condition of $\delta E = 0$. In the case of $\delta E \rightarrow 0$, HEROS-XES is transferred to RXES, and the condition: $E_{inc} = E_K$ is fulfilled. Therefore, the HEROS-XES spectra can be measured at several incidence energies far from resonances, and the thus obtained dataset is used to extrapolate towards E_K with high precision. Eqn (1) provides the linear relation between E_K–E_{M3}–E and incident beam energy for such excitation conditions. This behavior is shown in Fig. 3 for $FeCl_3$. The detuning parameter δE for XES is defined as the energy gap between the $FeCl_3$ Kβ mainline position and the determined HEROS-XES high energy cut-off $E_{cut-off}$; thus, $\delta E = E_{cut-off} - E_K + E_{M3}$. The HEROS-XES spectra are compared to the nXES spectrum recorded at an incident energy of 7300 eV. For an incident energy of 7113.7 eV that corresponds to resonant excitation into the 3d state, HEROS-XES is entirely substituted by the RXES spectrum of the $1s^2 3p^5 3d^4$ state (Fig. 3a, bottom). The nXES maximum is 7059.47 eV, while the RXES maximum arises at 7059.87 eV. A different final state and multielectron interaction can account for this variance.[28,34,59] We recognize the RXES $K\beta_{1,3}$ mainline position at the incidence of 7113.7 eV as the correct ionization threshold for the 3p 1s transition since it represents the first state populated by the photoionization event for the lowest incident energy, without additional energy transfer from the emitted photon.

HEROS is well described in terms of inelastic X-ray scattering. The energy conservation rule for the scattering process in the off-resonant region provides $E_K = E_{M3} + E_{cut-off} - \delta E$. To extrapolate absorption edge position the E_K, high quality RXES plane or sets of HEROS-XES spectra for different E_{inc} values are required to determine the $E_{cut-off}$ from their derivatives. Additionally, an RXES spectrum corresponding to the first unoccupied state is necessary. This state can be precisely determined based on the RXES plane measurement and extracted HERFD-XANES spectrum as shown in Fig. 4a, bottom. In this way, a first accessible unoccupied state defined by the relation $E_K - E_{M3}$ and not affected by energy transfer from the emitted photon will be characterized. The advantage of this approach is that the evolution of derivatives can be tracked with changing E_{inc} (see the ESI† for derivatives) in a fixed arrangement, and emission spectra are collected in an energy-dispersive mode, which offers superior resolution. The proposed solution will be highly advantageous, especially for the FEL experiments with a fixed setup: single-shot measurements, single-shot pump-probe experiments, and single-shot X-ray pump – X-ray probe experiments. While the X-ray spectrometers are operating at a relatively high diffraction order of the crystal, the energy resolution is superior to typical resolution for incidence beam monochromators working with Si(111) crystals. Additionally, the core-hole lifetime broadening due to the final state $3p^{n-1}4p^1$ is present.

The calibration scheme proposed in Fig. 3 can be expanded further to form a 2D calibration plane based on different compounds. Fig. 4a presents a 2D calibration plane for Fe^0–Fe^{III} compounds. For each HEROS-XES spectrum, a δE was computed and plotted as a function of the incident energy in the same way as shown in Fig. 3b. Linear relations were extrapolated to $\delta E = 0$ corresponding to the incident energy equal to E_0 in XAS. The universal relation for the E_1 value corresponding to any point on the calibration plane can be derived from simple geometry as:

$$\delta E = E_{inc} + \delta E^1 - E_{inc}{}^1 \quad (2)$$

where δE^1 is detuning at the corresponding incident energy $E_{inc}{}^1$ for a studied compound. Table 1 presents the results of the proposed procedure for all three studied compounds compared to the results obtained by classical methods. HEROS-XES derivatives are available in the ESI.† Note that there are no statistically significant differences between the HEROS-based and XAS-based calibration. For an XES spectrometer

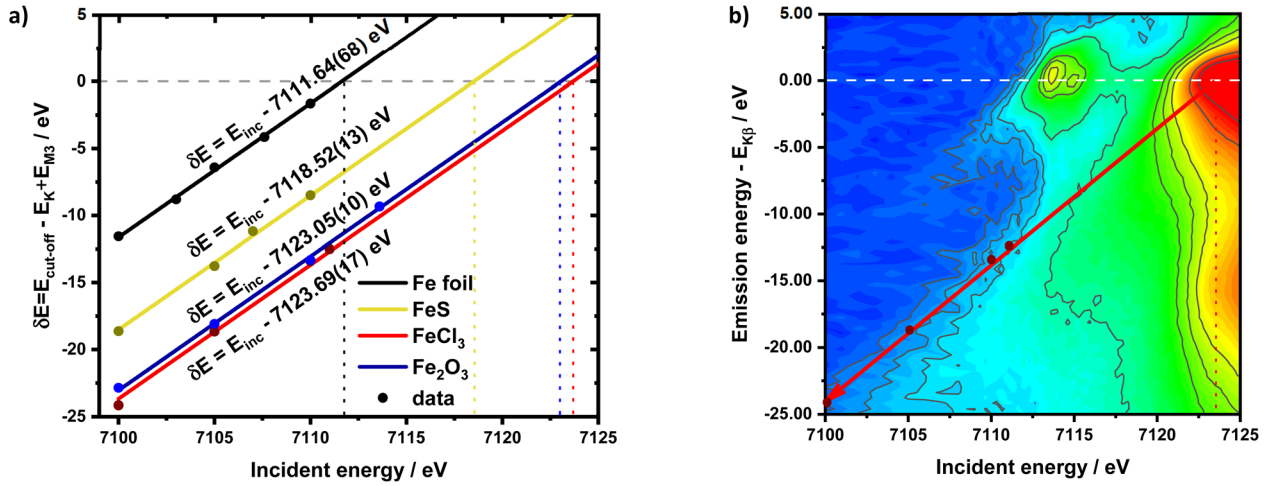

Fig. 4 (a) detuning parameter δE in the function of incident energy for different compounds along with fitted lines and corresponding equations. Vertical dotted lines indicate the obtained values of the absorption edge position while the horizontal dashed line marks $\delta E = 0$. (b) RXES plane for $FeCl_3$ with the HEROS cut-off position marked by the dark red arrow, the calibration points marked by red dots and E_0 marked by the vertical dashed line. The emission energy axis was scaled to match the condition $E_{K\beta} = 0$ and is marked by the horizontal dashed line.

Table 1 3p state energy derived using different methods

	E_{M3} energy [eV]		
Compound	XAS	HEROS	XPS
$FeCl_3$	63.06	64.22(17)	55.9[60]
α-Fe_2O_3	62.97	63.15(10)	55.6[61]
FeS	58.95	59.56(13)	53.8[62]
Fe foil	53.10	53.05(7)	52.9[63]

calibration, one must collect fluorescence from the reference metal foil for different incident energies around the absorption edge with a fixed emission bandwidth. With the HEROS-XES approach, three HEROS scans and a non-resonant XES spectrum are required to determine precise calibration without the need for reference foil. For extrapolated E_0 values, a classical calibration curve E_{inc}(formal oxidation state) can be plotted (see the ESI†). From the linear relation between the AOS (average oxidation state) *vs.* incident energy and eqn (2), an oxidation state formula can be obtained:

$$\mathrm{AOS} = \frac{E^1_{inc} - \delta E^1 - b}{a} \quad (3)$$

where $a = 7111.69$ eV and $b = 3.61$ eV^{-1} are the incident and slope of the E_{inc}(formal oxidation state) relation derived for E_K values from Fig. 4a and Table 1.

It is interesting to evaluate from KH formalism and eqn (1) the low energy limit for the scattering process, *i.e.*, the lowest incidence energy required to induce the off-resonant scattering process. The lowest incidence energy has to be equal to the energy of the final state (E_{M3}) from energy conservation. Thanks to this property, the obtained calibration curves for oxidation state determination can be employed to determine the energy of the final state by extrapolating the calibration curves to $E_{cutoff} = 0$. In Fig. 5, we show the obtained result used to extract the 3p final state (M3 edge) energies for the measured samples. The M3 energy values are shown in Table 1 and compared to the XPS data and the results extracted from high-resolution XAS measurements. For the latter, we used Kβ emission energy (3p → 1s) and subtracted the K energy that has been obtained from the inflection point of the absorption curves. There is clear evidence of the difference between X-ray and XPS data. This effect can be assigned to the penetration depths that can be achieved in both measurements. The measured signal in the XPS experiment contains a significant contribution of surface states mixed with bulk state information. In the case of X-rays, the penetration depth is in the range of a few microns, and the bulk properties of the material are probed. In this context, we should emphasize that only the X-ray spectroscopy methods can give insights into the high electronic orbitals with bulk sensitivity. The HEROS and XANES data comparison indicate small change in the eV range

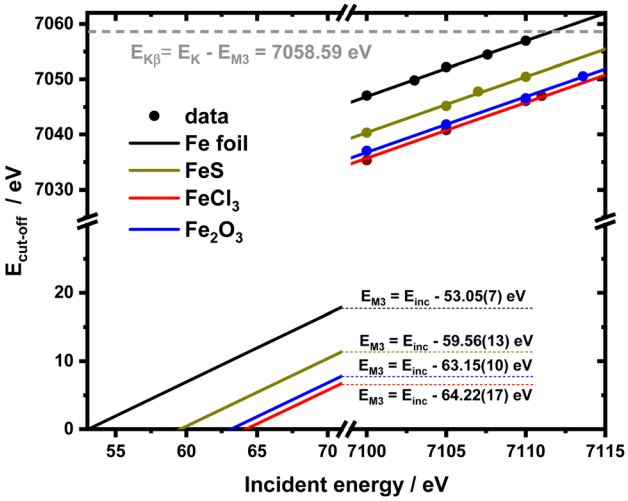

Fig. 5 2D calibration plane from figure recalculated for the absolute $E_{cut\text{-}off}$ values and extended till 0 to extrapolate E_M3 values.

for FeS and $FeCl_3$, while the obtained values for α-Fe_2O_3 and Fe are essentially the same. The difference may result from the interaction between the initial and final states with remaining electronic states, particularly 3p-3d exchange interaction.[29] Also, the E_{1s} edge position extracted from the XAS curve may not be precise enough as the near edge spectra are overlapped with resonant features. Furthermore, we should note the difference in the scheme of the scattering process. In non-resonant XES, the 1s core hole is filled within a 0.55 fs [57] lifetime, and this scattering time is constant, independent of the incidence energy. In the case of the off-resonant scattering process, the time of scattering equals:[64]

$$t_{vi} = \frac{\hbar}{\sqrt{(E_K - E_0)^2 + \Gamma_K^2}} \quad (4)$$

where $\hbar$ is a Dirac constant, and for incidence energies around 20 eV below the threshold, the scattering times are in the range of less than 0.05 fs. In this context, the interaction outcome of electronic states involved in transition with remaining electrons may be different due to the time dependency of the scattering cross-section.

Finally, we would like to point out that the absorption edge position or absorption threshold is not well defined.[43] According to the most popular experimental approach the absorption edge is composed of an atomic background, modelled by atan or erf functions convoluted with specific electronic transitions modelled by using Lorentzian or Voight functions.[15,43] By definition, the absorption edge starts when the incident energy is enough to promote transition of the core electron to a continuum.[43] However, absorption cross section can be derived directly from Fermi's golden rule written for X-ray absorption with wavefunctions for all electronic states used; thus, XANES involves bound states and a continuum. One can argue that the absorption threshold, especially in the context of the physical oxidation state, should be considered, where the first unoccupied states emerge, including pre-edge transitions. Such an understanding was already proven to be correct in the analysis of the composition of glasses[65,66] and minerals.[22,26] Here, we do not contest the definition of the absorption threshold or its relation to the physical oxidation state. Furthermore, since relation (2) is linear, the presented approach can be extended to any edge feature, including the pre-edge.

Conclusions

These results offer new physical oxidation state determination opportunities, which could be problematic based only on the XANES edge position. An ambiguity of this approach is recognized in the literature, for example, for Cr species.[7] The minimal requirement for a correct calibration curve is three different oxidation states, and the most suitable reference would be a single, neutral Me atom and separate Me^{2+} and Me^{3+} ions. With an apparent lack of perfect references, the most plausible references for the oxidation state analysis should be a metal foil as the Me^0 reference, MeF_2 for Me^{2+}, and MeF_3 for Me^{3+} since F is the most electronegative element in the periodic table. Alternatively, a proposed calibration scheme based on the relative positions of the HEROS cutoff and Kβ mainline maximum can establish a correct energy grid. The presented method allows for environment-independent E_0 determination at a given energy grid. As a consequence of the equivalence of HEROS and HERFD, with respect to the challenges in determining the edge position, the methods are the same. While the HEROS-based approach benefits from enhanced resolution of XES spectrometers, the $E_{cut\text{-}off}$ determination still is affected by noise in the derivatives of the spectra and restricted to elements with $Z > 20$. However, the same approach can be utilized to calibrate the energy scale at charge integrating detectors at FEL sources, where much more intense signals can be achieved. Although the proposed method would also test a linear dependence between the formal oxidation state and E_0, it is beyond the scope of the current communication.

The definition of the physical oxidation state remains ambiguous due to the problems with its precise determination, and this uncertainty raises several problems in physics and chemistry. We have demonstrated that using off-resonant XES spectroscopy, information about XAS E_K can be derived. HEROS-XES contains information about unoccupied DOS functions of an atom, and the spectra can be transformed into HEROS-XAS. The XAS-related detuning parameter δE does not affect the position of the HEROS-XAS edge (E_0) while the HEROS-XES edge ($E_0(E_{inc} - E_{M3} - E_{em})$) shifts linearly with the incident energy. This property can be used to derive a relation between the XES-related detuning parameter δE and E_0 to determine the absorption edge energy. The precise and unbiased absorption edge shape value of E_0 can help render the exact value of the oxidation state, which is a significant step closer to obtaining a well-defined oxidation state of an atom in a molecule. We should emphasize that the proposed methodology can be very relevant for studies of 3d-based metals (*e.g.* Ti, Cr, or Cu), metal-centered molecules important for biological research or nanomaterials as well as hybrid-systems important for renewable energy technologies. Importantly, application of X-rays allows for *in situ* research and for determination of electronic structure changes and the energy distribution of charges as a function of time with time-resolved pump-probe experiments at synchrotrons and X-ray free electron lasers. When using dispersive type spectrometers, the HEROS spectra may be recorded with single-shot and shot-to-shot modes without the need for scanning of any optical components of the beamline and end station. Moreover, the use of a stochastic self-amplified spontaneous emission process that delivers broadband X-ray spectra may be considered for application. High energy resolution for the latter may be maintained with recently developed reconstruction methods applied with SASE XFEL beams.[67]

Author contributions

Conceptualization: MN, JS, MB; data curation: MN, AK; formal analysis: MN; funding acquisition: MB; investigation: MN, AK, JS, RF, MB; methodology: MN; project administration: MN;

resources: MN, MB; software: AK; supervision: MB; validation: MN, AK, JS, RF, MB; visualization: MN; writing – original draft: MN, AK; writing – review & editing: MN, AK, JS, RF, MB.

Conflicts of interest

There are no conflicts to declare.

Acknowledgements

PETRA III at DESY and beamline P64 are acknowledged for the provision of beamtime. MN and MB acknowledge the German BMBF for funding in frame of project Syn-XAS (FKZ 05K18PPA) and FocusPP64 (FKZ05K19PP1). JS and RF acknowledge partial support from the National Science Centre (Poland) and their grant no. 2020/37/B/ST3/0055. The authors would like to thank dr. Wolfgang Caliebe (Petra III, DESY) for assistance.

Notes and references

1 S. Pehkonen, *Analyst*, 1995, **120**, 2655–2663.
2 J. J. Leani, H. J. Sánchez, M. Valentinuzzi and C. Pérez, *J. Anal. At. Spectrom.*, 2011, **26**, 378–382.
3 P. H. L. Sit, R. Car, M. H. Cohen and A. Selloni, *Inorg. Chem.*, 2011, **50**, 10259–10267.
4 L. Burkhardt, Y. Vukadinovic, M. Nowakowski, A. Kalinko, J. Rudolph, P. A. Carlsson, C. R. Jacob and M. Bauer, *Inorg. Chem.*, 2020, **59**, 3551–3561.
5 W. M. Kwiatek, M. Galka, a. L. Hanson, C. Paluszkiewicz and T. Cichocki, *J. Alloys Compd.*, 2001, **328**, 276–282.
6 K. K. Gunter, L. M. Miller, M. Aschner, R. Eliseev, D. Depuis, C. E. Gavin and T. E. Gunter, *Neurotoxicology*, 2002, **23**, 127–146.
7 M. Tromp, J. Moulin, G. Reid and J. Evans, *AIP Conf. Proc.*, 2007, **882**, 699–701.
8 F. de Groot, G. Vankó and P. Glatzel, *J. Phys. Condens. Matter*, 2009, **21**, 104207.
9 J. J. Rehr, *Rev. Mod. Phys.*, 2000, **72**, 621–654.
10 J. J. Ã. Rehr, *Radiat. Phys. Chem.*, 2006, **75**, 1547–1558.
11 M. Bauer and H. Bertagnolli, *Methods Phys. Chem.*, 2012, **1**, 231–269.
12 R. G. Shulman, Y. Yafet, P. Eisenberger and W. E. Blumberg, *Proc. Natl. Acad. Sci.*, 1976, **73**, 1384–1388.
13 J. A. Kirby, D. B. Goodin, T. Wydrzynski, A. S. Robertson and M. P. Klein, *J. Am. Chem. Soc.*, 1981, **103**, 5537–5542.
14 C. R. Natoli, *Springer Proc. Phys.*, 1984, **13**, 38–42.
15 J. Stöhr, in *NEXAFS Spectroscopy*, ed. H. K. V. Lotsch, G. Ertl, R. Gomer and D. L. Mills, Springer-Verlag Berlin Heidenberg, Berlin, 2nd edn, 1996, pp. 211–238.
16 M. Bauer, *Phys. Chem. Chem. Phys.*, 2014, **16**, 13827–13837.
17 J. Rabeah, M. Bauer, W. Baumann, A. E. C. McConnell, W. F. Gabrielli, P. B. Webb, D. Selent and A. Brückner, *ACS Catal.*, 2013, **3**, 95–102.
18 R. Grauke, R. Schepper, J. Rabeah, R. Schoch, U. Bentrup, M. Bauer and A. Brückner, *ChemCatChem*, 2019, 1025–1035.
19 P. Glatzel and U. Bergmann, *Coord. Chem. Rev.*, 2005, **249**, 65–95.
20 S. Datta, A. M. Rule, J. N. Mihalic, S. N. Chillrud, B. C. Bostick, J. P. Ramos-Bonilla, I. Han, L. M. Polyak, A. S. Geyh and P. N. Breysse, *Environ. Sci. Technol.*, 2012, **46**, 3101–3109.
21 S. H. Lee, I. Sullivan, D. M. Larson, G. Liu, F. M. Toma, C. Xiang and W. S. Drisdell, *ACS Catal.*, 2020, **10**, 8000–8011.
22 A. J. Berry, G. M. Yaxley, A. B. Woodland and G. J. Foran, *Chem. Geol.*, 2010, **278**, 31–37.
23 M. Wilke, O. Hahn, A. B. Woodland and K. Rickers, *J. Anal. At. Spectrom.*, 2009, **24**, 1364.
24 A. Boubnov, H. Lichtenberg, S. Mangold and J. D. Grunwaldt, *J. Synchrotron Radiat.*, 2015, **22**, 410–426.
25 E. Cottrell, K. a. Kelley, A. Lanzirotti and R. a. Fischer, *Chem. Geol.*, 2009, **268**, 167–179.
26 M. Wilke, F. Farges, P. E. Petit, G. E. Brown and F. Martin, *Am. Mineral.*, 2001, **86**, 714–730.
27 N. Lee, T. Petrenko, U. Bergmann, F. Neese and S. Debeer, *J. Am. Chem. Soc.*, 2010, **132**, 9715–9727.
28 G. Vankó, T. Neisius, G. Molnár, F. Renz, S. Kárpáti, A. Shukla and F. M. F. De Groot, *J. Phys. Chem. B*, 2006, **110**, 11647–11653.
29 M. Pollock, U. Delgado-Jaime, M. Atanasov, F. Neese and S. Debeer, *J. Am. Chem. Soc.*, 2014, **136**, 9453–9463.
30 G. Peng, X. Wang, C. R. Randall, J. A. Moore and S. P. Cramer, *Appl. Phys. Lett.*, 1994, **65**, 2527–2529.
31 J. A. Rees, A. Wandzilak, D. Maganas, N. I. C. Wurster, S. Hugenbruch, J. K. Kowalska, C. J. Pollock, F. A. Lima, K. D. Finkelstein and S. DeBeer, *J. Biol. Inorg Chem.*, 2016, **21**, 793–805.
32 H. Visser, E. Anxolabéhère-Mallart, U. Bergmann, P. Glatzel, J. H. Robblee, S. P. Cramer, J.-J. Girerd, K. Sauer, M. P. Klein and V. K. Yachandra, *J. Am. Chem. Soc.*, 2001, **123**, 7031–7039.
33 G. Tirao, S. Ceppi, A. L. Cappelletti and E. V. Pannunzio Miner, *J. Phys. Chem. Solids*, 2010, **71**, 199–205.
34 R. G. Castillo, A. W. Hahn, B. E. Van Kuiken, J. T. Henthorn, J. McGale and S. DeBeer, *Angew. Chem.*, 2021, **133**, 10200–10209.
35 J. Kowalska and S. DeBeer, *Biochim. Biophys. Acta, Mol. Cell Res.*, 2015, **1853**, 1406–1415.
36 F. M. F. De Groot, P. Glatzel, U. Bergmann, P. A. Van Aken, R. A. Barrea, S. Klemme, M. Hävecker, A. Knop-Gericke, W. M. Heijboer and B. M. Weckhuysen, *J. Phys. Chem. B*, 2005, **109**, 20751–20762.
37 A. Kotani and S. Shin, *Rev. Mod. Phys.*, 2001, **73**, 203–246.
38 P. Glatzel, M. Sikora, G. Smolentsev and M. Fernández-García, *Catal. Today*, 2009, **145**, 294–299.
39 L. J. P. Ament, M. Van Veenendaal, T. P. Devereaux, J. P. Hill and J. Van Den Brink, *Rev. Mod. Phys.*, 2011, **83**, 705–767.
40 M. Nowakowski, J. Czapla-Masztafiak, J. Szlachetko and W. M. Kwiatek, *Chem. Phys.*, 2017, **493**, 49–55.
41 J. P. Rueff and A. Shukla, *Rev. Mod. Phys.*, 2010, **82**, 847–896.
42 C. J. Milne, T. J. Penfold and M. Chergui, *Coord. Chem. Rev.*, 2014, **277–278**, 44–68.
43 C. T. Chantler, *Int. Tables Crystallogr.*, 2021, 1–9.
44 W. A. Caliebe, V. Murzin, A. Kalinko and M. Görlitz, *AIP Conf. Proc.*, 2019, **2054**, 060031.

45 A. Kalinko, W. A. Caliebe, R. Schoch and M. Bauer, *J. Synchrotron Radiat.*, 2020, **27**, 31–36.
46 H. Hayashi, R. Takeda, Y. Udagawa, T. Nakamura, H. Miyagawa, H. Shoji, S. Nanao and N. Kawamura, *Phys. Scr., T*, 2005, **115**, 1094–1096.
47 H. Hayashi, R. Takeda, Y. Udagawa, T. Nakamura, H. Miyagawa, H. Shoji, S. Nanao and N. Kawamura, *Phys. Rev. B: Condens. Matter Mater. Phys.*, 2003, **68**, 1–9.
48 J. Szlachetko, J. C. Dousse, M. Berset, K. Fennane, M. Szlachetko, J. Hoszowska, R. Barrett, M. Pajek and A. Kubala-Kukus, *Phys. Rev. A: At., Mol., Opt. Phys.*, 2007, **75**, 1–11.
49 W. Błachucki, J. Szlachetko, J. Hoszowska, J. C. Dousse, Y. Kayser, M. Nachtegaal and J. Sá, *Phys. Rev. Lett.*, 2014, **112**, 1–5.
50 W. Błachucki, J. Hoszowska, J. C. Dousse, Y. Kayser, R. Stachura, K. Tyrała, K. Wojtaszek, J. Sá and J. Szlachetko, *Spectrochim. Acta, Part B*, 2017, **136**, 23–33.
51 J. Szlachetko, M. Nachtegaal, J. Sá, J. Dousse, J. Hoszowska, E. Kleymenov, M. Janousch, O. Safonova, C. König and J. van Bokhoven, *Chem. Commun.*, 2012, **48**, 10898–10900.
52 I. Pudza, A. Kalinko, A. Cintins and A. Kuzmin, *Acta Mater.*, 2021, **205**, 116581.
53 J. Tulkki and T. Aberg, *J. Phys. B At. Mol.*, 1982, **15**, L435–L440.
54 T. Åberg and J. Tulkki, in *Atomic Inner-Shell Physics*, ed. B. Crasemann, Plenum, New York, Springer, Boston, MA, Boston, 1985, pp. 419–463.
55 P. Eisenberger, P. M. Platzman and H. Winick, *Phys. Rev. Lett.*, 1976, **36**, 623–626.
56 J. Szlachetko and Y. Kayser, in *High-Resolution XAS/XES: Analyzing Electronic Structures of Catalysts*, ed. J. Sá, CRC Press, Boca Raton, 2014, pp. 59–116.
57 J. L. Campbell and T. Papp, *At. Data Nucl. Data Tables*, 2001, **77**, 1–56.
58 M. L. Berger, J. Hubbell, S. Seltzer, J. Chang, J. Coursey, R. Sukumar, D. Zucker, K. Olsen, *NIST Standard Reference Database 8 (XGAM)*, 2010.
59 G. Vanko, A. Bordage, P. Glatzel, E. Gallo, M. Rovezzi, W. Gawelda, A. Galler, C. Bressler, G. Doumy, A. M. March, E. P. Kanter, L. Young, S. H. Southworth, S. E. Canton, J. Uhlig, G. Smolentsev, V. Sundstrom, K. Haldrup, T. B. Van Driel, M. M. Nielsen, K. S. Kjaer and H. T. Lemke, *J. Electron Spectrosc. Relat. Phenom.*, 2013, **188**, 166–171.
60 J. Wang, B. Mao, M. G. White, C. Burda and J. L. Gole, *RSC Adv.*, 2012, **2**, 10209–10216.
61 T. Yamashita and P. Hayes, *Appl. Surf. Sci.*, 2008, **254**, 2441–2449.
62 K. Shimada, T. Mizokawa, K. Mamiya, T. Saitoh, A. Fujimori and T. Kamimura, *Surf. Sci. Spectra*, 1999, **6**, 321–336.
63 P. Mills and J. L. Sullivan, *J. Phys. D. Appl. Phys.*, 1983, **16**, 723–732.
64 F. Gelmukhanov, P. Sałek, T. Privalov and H. Ågren, *Phys. Rev. A: At., Mol., Opt. Phys.*, 1999, **59**, 380–389.
65 F. Farges, Y. Lefrère, S. Rossano, A. Berthereau, G. Calas and G. E. Brown, *J. Non. Cryst. Solids*, 2004, **344**, 176–188.
66 F. Farges, S. Rossano, Y. Lefrre, M. Wilke and G. E. Brown Jr, *Phys. Scr.*, 2005, **T115**, 957–959.
67 Y. Kayser, C. Milne, P. Juranić, L. Sala, J. Czapla-Masztafiak, R. Follath, M. Kavčič, G. Knopp, J. Rehanek, W. Błachucki, M. G. Delcey, M. Lundberg, K. Tyrała, D. Zhu, R. Alonso-Mori, R. Abela, J. Sá and J. Szlachetko, *Nat. Commun.*, 2019, **10**, 1–10.